Observations of the Surf-Zone Turbulent Dissipation Rate

FALK FEDDERSEN

Scripps Institution of Oceanography, University of California, San Diego, La Jolla, California

(Manuscript received 26 April 2011, in final form 3 October 2011)

ABSTRACT

The contributions of surface (breaking wave) boundary layer (SBL) and bottom (velocity shear) boundary layer (BBL) processes to surf-zone turbulence is studied here. The turbulent dissipation rate ϵ, estimated on a 160-m-long cross-shore instrumented array, was an order of magnitude larger within the surf zone relative to seaward of the surf zone. The observed ϵ covaried across the array with changing incident wave height, tide level, and alongshore current. The cross-shore-integrated depth times ϵ was correlated with, but was only 1% of, the incident wave energy flux, indicating that surf-zone water-column turbulence is driven directly (turbulence injected by wave breaking) or indirectly (by forcing alongshore currents) by waves and that the bulk of ϵ occurs in the upper water column. This small fraction is consistent with laboratory studies. The surf-zone-scaled (or Froude-scaled) ϵ is similar to previous field observations, albeit somewhat smaller than laboratory observations. A breaking-wave ϵ scaling is applicable in the midwater column at certain locations, indicating a vertical diffusion of turbulence and ϵ balance. However, observations at different cross-shore locations do not collapse, which is consistent with a cross-shore lag between wave energy gradients and the surface turbulence flux. With strong alongshore currents, a BBL-scaled ϵ indicates that shear production is a significant turbulence source within the surf zone, particularly in the lower water column. Similarly for large currents at one location, the dissipation to shear production ratio approaches one. Both dissipation scalings depend upon wave energy flux gradients. The ratio of BBL to SBL ϵ has complex dependencies but is larger for a deeper part of the surf zone and more obliquely incident waves.

1. Introduction

The surf zone, where depth-limited breaking occurs, is shallow (<4 m depth, depending upon wave height). Surf-zone water-column turbulence, generated by both wave breaking and vertical shear in the alongshore current, vertically mixes momentum, sediment, biota, and tracer. However, surf-zone turbulence energetics are not well understood.

In unstratified boundary layers where the vertical length scale is much less than the horizontal length scale, the turbulence energetics often are simplified to a steady-state balance of shear production P, vertical diffusion of turbulent kinetic energy (TKE) k, and the turbulent dissipation rate ϵ: that is,

$$P + \frac{d}{dz}\left(\nu \frac{dk}{dz}\right) - \epsilon = 0, \tag{1}$$

where z is the elevation above the bed and ν is TKE eddy diffusivity. Horizontal advection of TKE gradients are assumed negligible. Well seaward of the surf zone, turbulence is typically separated into two boundary layer regimes. The first is near the bed within the bottom boundary layer (BBL), where turbulence is driven by wall-bounded shear, and the second is the surface boundary layer (SBL) typically driven by wave breaking. In sufficiently deep water, these two boundary layer regions are distinct. However, in the shallow surf zone, the two boundary layer regions can overlap.

Within a general BBL, turbulence is generated by vertical shear of the mean flow; $P = \epsilon$ is the dominant turbulence balance in (1), resulting in a velocity "log layer" and a dissipation scaling of

$$\epsilon = \frac{u_*^3}{\kappa z}, \tag{2}$$

where u_* is the bed friction velocity and $\kappa \approx 0.4$ is the empirical Von Kármán constant. The friction velocity is defined so that ρu_*^2 is the bottom stress, where ρ is the

Corresponding author address: F. Feddersen, Scripps Institution of Oceanography, 9500 Gilman Dr., La Jolla, CA 92093-0209.
E-mail: falk@coast.ucsd.edu

DOI: 10.1175/JPO-D-11-082.1

water density. This scaling assumes a turbulent macro length scale that increases linearly with z with slope κ (i.e., $l = \kappa z$). Grant and Madsen (1979) extended these concepts to include the presence of wave-orbital velocities. The BBL concept has been applied in many non-surf-zone geophysical settings. In tidal, continental shelf, estuarine, and coral reef BBLs without surface gravity waves, the BBL ϵ scaling [(2)] or $P = \epsilon$ (or both) applied within 3 m above the bed (e.g., Gross and Nowell 1985; Dewey and Crawford 1988; Sanford and Lien 1999; Trowbridge et al. 1999; Peters and Bokhorst 2000; Reidenbach et al. 2006). A BBL TKE balance that included stratification-induced buoyancy flux closed within 2 m of the bed on the continental shelf in 60-m water depth with energetic surface gravity waves (Shaw et al. 2001). In a tidal estuary with strong winds and whitecapping waves and strong currents, the observed near-bed ($\leq$0.5 m) ϵ was consistent with (2) (Jones and Monismith 2008a).

Seaward of the surf zone, in the unstratified SBL, whitecapping wave breaking is the dominant turbulence source at depths up to several times the significant wave height in deep water (e.g., Agrawal et al. 1992). Under whitecapping conditions, Terray et al. (1996) showed that observed near-surface dissipation scaled as

$$\frac{\epsilon H_s}{G} = A\left(\frac{z'}{H_s}\right)^{\lambda}, \tag{3}$$

where z' is the distance from the surface and H_s is the significant wave height, A is a constant, λ is a power-law exponent, and G is the whitecapping-induced surface TKE flux parameterized to depend upon the wind stress and the wave growth rates (e.g., Craig and Banner 1994; Terray et al. 1996). The canonical value $\lambda = -2$ found by Terray et al. (1996) has been approximately observed in other SBL environments with whitecapping wave breaking. This includes the open ocean (Drennan et al. 1996; Soloviev and Lukas 2003), a lake (Stips et al. 2005), and the middle to upper part of the water column in the nearshore region offshore of the surf zone (Feddersen et al. 2007; Gerbi et al. 2009) and in the upper water column of a tidal estuary with strong winds and whitecapping waves (Jones and Monismith 2008a). Many of these studies also measured $P \ll \epsilon$ (Feddersen et al. 2007; Gerbi et al. 2009). Note, that for open-ocean interacting sea and swell, ϵ did not follow the Terray scaling (Greenan et al. 2001). The departure from surface log-layer ($\epsilon \sim z'^{-1}$) scaling implies that vertical turbulent diffusion balances dissipation [$d/dz(\nu dk/dz) = \epsilon$], but measuring turbulent diffusion in the field SBL is extremely challenging. With an appropriate choice of the surface length scale, two-equation turbulence models (e.g., k–ϵ and k–ω), with length scale $l \propto z'$, reproduce the scaling (3) with $\lambda \approx -2$ (e.g., Burchard 2001; Umlauf et al. 2003; Jones and Monismith 2008b).

Within the surf-zone SBL, depth-limited wave breaking is a significant turbulent source. Furthermore, surf-zone alongshore currents V can be strong, as large as 1.5 m s^{-1} (Feddersen and Guza 2003, and others), resulting in large u_* and potentially strong BBL-generated turbulence. Thus, within the surf zone the SBL [d/dz ($\nu dk/dz$) = ϵ] and BBL ($P = \epsilon$) regions likely overlap, resulting in a potentially complex turbulence environment within the water column that is not well understood.

Within the natural surf zone, turbulence measurements are sparse. Hot-film anemometer-based surf-zone turbulent dissipation rate ϵ varied between 5×10^{-5} and 5×10^{-2} m^2 s^{-3} (George et al. 1994, hereafter GFG), and acoustic Doppler velocimeter (ADV)-based surf-zone ϵ varied between 10^{-5} and 10^{-3} m^2 s^{-3} (Bryan et al. 2003, hereafter BBG). Combining these two datasets from two different beaches with different conditions and methods, the nondimensionalized surf-zone-scaled dissipation $\epsilon/(g^3h)^{1/2}$ had similar nondimensional depth z/h dependence (Feddersen and Trowbridge 2005). Within the swash zone ($h < 0.25$ m), ADV-estimated values of ϵ as large as 10^{-1} m^2 s^{-3} have been reported (Raubenheimber et al. 2004). In 4.5-m water depth during active wave-breaking conditions ($H_s > 1.8$ m), $\epsilon \approx 10^{-4}$ m^2 s^{-3} and shear production balanced ϵ at $z = 1$ m above the bed (Trowbridge and Elgar 2001), with no indication of breaking-wave-enhanced ϵ as expected under deep-water wave breaking (e.g., Agrawal et al. 1992; Terray et al. 1996). However, during these periods, the strong mean alongshore currents ($|V| >$ 1 m s^{-1}) induced large bed shear stress, which resulted in BBL processes dominating SBL processes (Feddersen and Trowbridge 2005). The near-bed alongshore component of the turbulent Reynolds stress was consistent with BBL turbulence generation (Ruessink 2010).

In contrast to the few field observations, there are many laboratory surf-zone turbulence studies that span a range of scales (bed slopes varying from 1:10 to 1:35, wave heights varying from a few centimeters to 0.6 m, and wave periods from 1 to 4 s) using a variety of measurement techniques (e.g., Nadaoka et al. 1989; Ting and Kirby 1995; Chang and Liu 1999; Mocke 2001; Scott et al. 2005; Sou et al. 2010, and many others). More recently, laboratory turbulent dissipation rate ϵ has been directly estimated from the observed spatial velocity derivatives. For example, Govender et al. (2004) found that the majority of ϵ occurred above trough level. Kimmoun and Branger (2007) measured the wave-phase variation of ϵ across the surf zone. Huang et al. (2009) made phase-averaged (over a wave cycle) ϵ measurements from the

bed into the wave crest across the surf zone capturing the ϵ evolution from incipient wave breaking to run up. For 0.03-m incident wave heights, maximum instantaneous $\epsilon = 0.02\ \mathrm{m^2\ s^{-3}}$ was observed. Yoon and Cox (2010) measured the ϵ vertical structure using ADVs on a field-scale laboratory barred beach. Across a number of laboratory studies and varying wave heights, below trough level $\epsilon/(g^3h)^{1/2}$ largely collapses as a function of z/h (Ting and Kirby 1996; Govender et al. 2004; Huang et al. 2009; Yoon and Cox 2010) and is consistent with field surf-zone observations.

A critical aspect missing in laboratory surf-zone turbulence studies is the alongshore current V. Thus, nearly all laboratory surf-zone turbulence must be due to wave breaking (i.e., the SBL) and not the BBL. Note that the surf-zone energy lost in the near-bed wave boundary layer on a sandy beach is orders of magnitude less than that due to wave breaking (e.g., Thornton and Guza 1983). Within the water column (below trough level), where the majority of momentum, sediment, pollution, or biota is vertically mixed, the relative importance of surface and bottom boundary layer processes is not well understood.

Here, field surf-zone dissipation ϵ observations, estimated from a cross-shore ADV array (section 2), are examined. The observed ϵ cross-shore structure and variability are described in section 3. Cross-shore-integrated alongshore momentum and turbulent energy balances (section 4) indicate quasi-alongshore uniform conditions and yield bottom stress estimates and the fraction of observed wave energy flux dissipated, respectively. Local dissipation scalings, which require alongshore uniformity, are examined at individual surf-zone frames in section 5. Within the surf zone, the surf-zone-scaled dissipation $\epsilon/(g^3h)^{1/2}$ has a z/h dependence similar to previous field observations. Both surf-zone-adapted Terray scaling [(3)] and BBL [(2)] ϵ scalings are tested in the lower and mid water columns of the surf zone. Finally, a $P = \epsilon$ turbulent balance is tested at a single location that fluctuates between being within and seaward of the surf zone. Examination of these scalings provides insight into the turbulence dynamics within the water column (below trough level) as discussed in section 6. The results are summarized in section 7.

2. The HB06 field experiment and observations

Surf-zone field observations were collected during fall 2006 at Huntington Beach, California, state park (33.636°N, −117.969°E) as part of the HB06 experiment (Spydell et al. 2009; Clark et al. 2010; Feddersen 2010; Omand et al. 2011). The cross-shore coordinate x increases positively offshore with $x = 0$ m at the mean shoreline. The bathymetry was typically steep on the foreshore ($x \leq 25$ m), with a terraced midsection (30 m $< x <$ 70 m), and was steeper offshore (Fig. 1). At times, a small trough developed near $x = 50$ m. Seven instrumented tripod frames were deployed on a cross-shore transect spanning 160 m from near the shoreline to 4-m mean water depth (Fig. 1). The tripod frames (see Fig. 2 of Elgar et al. 2005) were oriented so that there are no flow obstacles for cross-shore-propagating waves and the alongshore current. Frames are numbered from F1 (shallowest) to F7 (deepest). Frame F2 (not shown) was often nonoperational and is not included in this analysis. At each frame, the vertical coordinate z is positive upward with $z = 0$ m at the bed. The instrument frames were leveled with possible orientation errors of ±3°. The tide range was ±0.5 m. Data were collected for 800 h from 14 September to 17 October 2006.

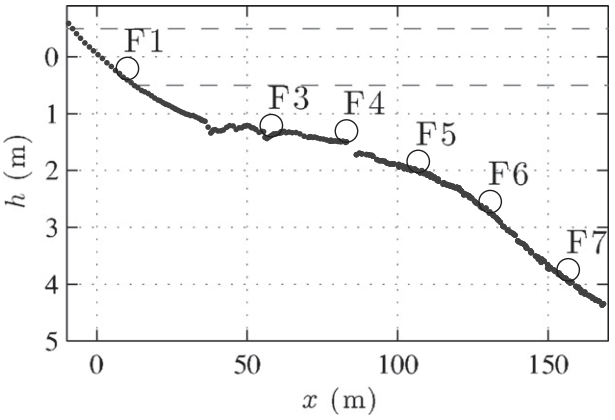

FIG. 1. Depth h vs cross-shore coordinate x. The instrument frame locations (circles) are denoted F1–F7. Frame F2 was often nonoperational and is not considered here. The horizontal dashed lines show the tide range std dev.

Each instrumented frame had a buried pressure sensor and downward-looking 5-MHz Sontek ocean ADV (Sontek 2004), both sampling at 8 Hz. Vertical instrument locations were GPS measured with errors of a few centimeters. The ADV measures three components of velocity (u, v, and w) aligned with the coordinate system. The velocity range was set to $\pm 5\ \mathrm{m\ s^{-1}}$, and velocities beyond this range (i.e., phase wrapping) were not observed. In each hourly data run, the ADV sampled 24 578 data points (51.2 min or 3072 s) and, for the remainder of the hour, went into bottom-finding mode to estimate ADV transducer height above the sea bed and (with mean pressure) water depth h. The ADVs were occasionally raised or lowered on the frames, as the sea bed eroded and accreted. The ADV sensing volume height above the bed varied, for F1–F4 between 0 and 0.4 m and for F5–F7 between 0.5 and 0.8 m. Data runs with sensing volume too close to the bed (≤0.03 m) are rejected. For each ADV hourly data run, surf-zone

ADV quality control (QC) methodology (Elgar et al. 2005), which rejects velocity data points when the ADV signal strength or correlation is low, is applied for calculation of wave and circulation statistics.

Hourly sea surface elevation spectra $P_{\eta\eta}$, calculated from the pressure sensor data, are used to estimate significant wave height H_s over the sea-swell (0.05–0.3 Hz) frequency band. Data from buried pressure sensors are adjusted following Raubenheimber et al. (1998). Assuming nonreflective, normally incident waves and integrating over the sea-swell band (0.05–0.3 Hz), the onshore wave energy flux F is estimated at each frame solely from pressure via

$$F = g\int_{0.05\,\mathrm{Hz}}^{0.3\,\mathrm{Hz}} P_{\eta\eta}(f)c_g(f)\,df, \tag{4}$$

where g is the gravitation constant and c_g is the linear-theory group velocity. These wave energy flux estimates (4) are consistent with estimates derived from combined pressure and ADV data that take into account nonnormal wave incidence and reflection (Sheremet et al. 2005). However, the pressure plus ADV–based F estimates are not independent of ADV data quality and thus are not used. Wave energy flux gradients dF/dx are estimated at F1–F6 by differencing F estimates from the neighboring onshore and offshore instruments, where, for F1, $F = 0$ is assumed at the shoreline. At F7, the off-diagonal radiation stress term S_{xy}/ρ is estimated from the spectra and directional moments (Kuik et al. 1988) derived from the pressure plus ADV data. At each frame, the hourly-mean alongshore current V and the time-averaged quadratic velocity product $\langle|\mathbf{u}|v\rangle$ are estimated, where $\mathbf{u}$ is the instantaneous horizontal velocity vector, and here $\langle\ \rangle$ represents a time average over the hour-long data run. If the Elgar et al. (2005) quality control criterion considered more than 40% of the data as bad, then the V and $\langle|\mathbf{u}|v\rangle$ estimates are rejected.

The ''break point'' location x_b, the seaward boundary of the surf zone, is estimated as the cross-shore frame where the onshore wave energy flux is <0.9 of the incident F7 energy flux, which is similar to choosing x_b as the location of maximum H_s. A frame is considered within the surf zone if located at or onshore of x_b and if the ratio $H_s/h \geq 0.4$ (Ruessink 2010). The H_s/h criterion is applied because at times a small trough had developed near F3, causing wave breaking, which is initiated farther offshore, to cease. Note that the boundary between the surf zone and region seaward is not sharp because, with random waves, the probability of breaking varies over a cross-shore region, from zero probability at some deeper offshore location to a probability of 1 at some shallow onshore location (e.g., Thornton and Guza 1983).

An upward-looking Nortek Aquadopp acoustic Doppler current profiler (ADCP) deployed at F5 (Fig. 1) provided vertical current structure at one location. The Aquadopp transducer face was located between 0.15 and 0.3 m above the bed as it accreted and eroded. The Aquadopp sampled 1-min-averaged u and v as a function of z with a vertical bin size of $\Delta z = 0.3$ m. The F5 ADV sensing volume was always between the first and second Aquadopp vertical bins. When linearly interpolated onto the height of the ADV sensing volume, the Aquadopp and ADV hourly estimated V agree well [root-mean-square (rms) error < 0.025 m s^{-1}, least squares best-fit slope of 1.04, and squared correlation $r^2 = 0.99$].

For hourly ADV data run, the turbulent dissipation rate ϵ is estimated from the high-frequency vertical velocity spectra $P_{ww}(f)$ (where f is frequency) with the Lumley and Terray (1983) model that converts a wavenumber k to a frequency spectrum for frozen turbulence in a mixed wave and mean current environment in the presence of a turbulent inertial subrange. Variants of this method have been used to estimate surf zone and nearshore ϵ (Trowbridge and Elgar 2001; BBG; Feddersen et al. 2007; Gerbi et al. 2009; Feddersen 2010). ADV vertical velocity spectra $P_{ww}(f)$ are calculated from the quality controlled (Feddersen 2010) vertical-velocity time series using 70-s-long data segments (detrended and Hanning windowed with 50% overlap). The turbulent dissipation rate ϵ is estimated from the velocity spectrum via (e.g., Feddersen et al. 2007)

$$\epsilon = \left\langle \left[\frac{P_{ww}(f)2(2\pi)^{3/2}}{\alpha M_{ww}(f;\overline{\mathbf{u}},\sigma^2_{u,v,w})} \right]^{3/2} \right\rangle, \tag{5}$$

where $\alpha = 1.4$ is Kolmogoroff's constant, $\overline{\mathbf{u}}$ and $\sigma^2_{u,v,w}$ are the horizontal mean current and (wave dominated) three-component velocity variance, M_{ww} is an integral over 3D wavenumber space that transforms the inertial-subrange $k^{-5/3}$ wavenumber dependence to frequency (Trowbridge and Elgar 2001; Feddersen et al. 2007), and here $\langle\rangle$ represents a frequency average between 1.2 and 2 Hz over 56 discrete frequencies. The ϵ estimates from (5) are rejected if the vertical velocity spectra power-law exponent or the ratio of horizontal to vertical spectra is inconsistent with an inertial subrange of turbulence (Feddersen 2010). Because of the long vertical pipes of the frame, any frame-generated wake turbulence is unlikely to pass these tests. This results in more rejected ϵ data runs at locations and times with strong wave breaking and when high in the water column. For the 800 h of observation, ϵ could be estimated 33% (at F1), 57% (at F3), 50% (at F4), 71% (at F5), 76% (at F6), and 70% (at F7) of the time.

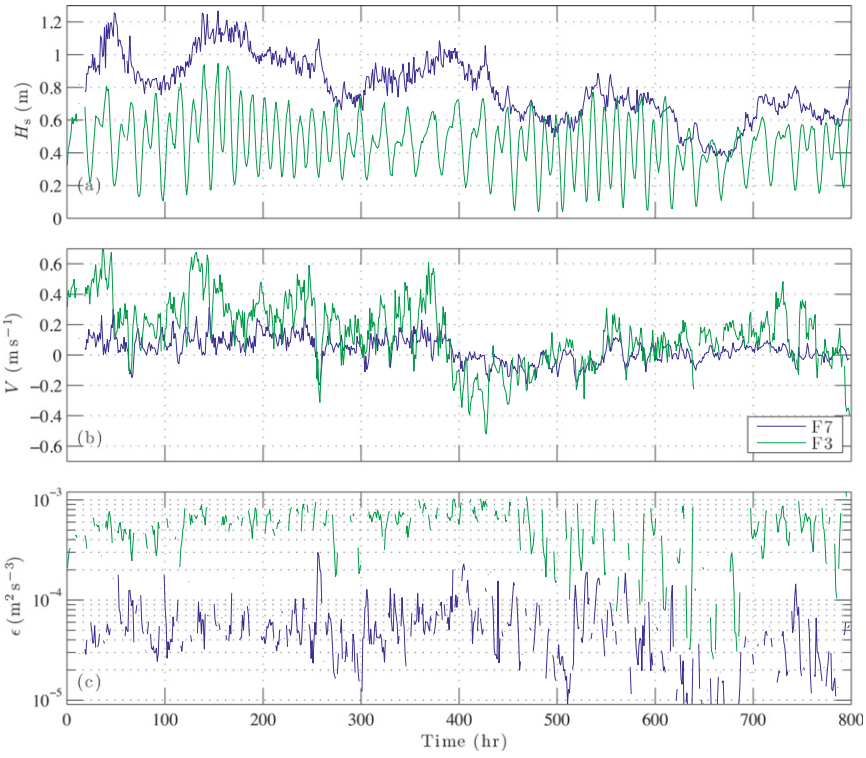

FIG. 2. (a) Significant wave height H_s, (b) mean alongshore current V, and (c) turbulent dissipation rate ϵ vs time at F7 (blue) and F3 (green). F7 was always located seaward of the surf zone, and F3 generally was located within the surf zone. Positive V is toward the northwest. In (c), ϵ gaps are times when the ADV was out of the water or failed the ϵ QC tests (Feddersen 2010).

3. Surf-zone dissipation variability

The incident F7 H_s varied between 0.4 and 1.2 m (Fig. 2a), the mean period varied between 8 and 13 s (not shown), and the mean wave angle (Kuik et al. 1988) varied between $+13°$ and $-10°$ (positive angles correspond to waves from the south; not shown). Larger H_s events corresponded to remotely (Southern Hemisphere) generated long-period swell with positive wave angles. At F3, H_s often was reduced relative to F7 because of tidally modulated depth-limited wave breaking (green curve in Fig. 2a), and thus, by definition, F3 usually was located within the surf zone. The break point location x_b varied between F3 and F6. Within the surf zone, the obliquely incident breaking waves drove (generally northward) alongshore current V of up to 0.7 m s^{-1} (green curve in Fig. 2b), which was tidally modulated (e.g., Thornton and Kim 1993). Seaward of the surf zone, the mean alongshore current V generally was weaker than within the surf zone (usually $|V| < 0.15$ m s^{-1}; blue curve in Fig. 2b).

Over the entire array, ϵ varied from 2×10^{-6} (at F7) to 3×10^{-3} m^2 s^{-3} (at F4). Typically, surf-zone ϵ varied between 10^{-4} and 10^{-3} m^2 s^{-3} (F3 in Fig. 2c). The observed surf-zone ϵ range is consistent with the previously observed range of Trowbridge and Elgar (2001) and BBG but is somewhat smaller than the range observed by GFG. The seaward of the surf-zone ϵ values are generally a factor of 10 smaller than for typical surf-zone ϵ (cf. blue and green curves for times 0–450 h in Fig. 2c). The F3 (typically surf zone) ϵ generally increases with larger incident H_s and is also tidally modulated increasing with lower tide (Fig. 2a).

The mean and standard deviation (std dev) of ϵ varied across the array. Because ϵ is not Gaussian distributed, a logarithmic (time average) mean dissipation $\overline{\epsilon} = \exp[\langle \log(\epsilon) \rangle]$ is calculated using all good ϵ estimates at each frame, and here $\langle\rangle$ denotes a time average. The logarithmic standard deviation of ϵ (σ_ϵ) is estimated similarly. At F6 and F7 (generally seaward of the surf zone), $\overline{\epsilon} \approx 4.5 \times 10^{-5}$ m^2 s^{-3}, increases shoreward to a F3 maximum of $\overline{\epsilon} = 4 \times 10^{-4}$ m^2 s^{-3}, and decreases slightly to $\overline{\epsilon} = 1.8 \times 10^{-4}$ m^2 s^{-3} at F1 (Fig. 3a). The logarithmic standard deviation of ϵ is about 1/3 of an order of magnitude and is approximately uniform across the array (width of dashed lines in Fig. 3a).

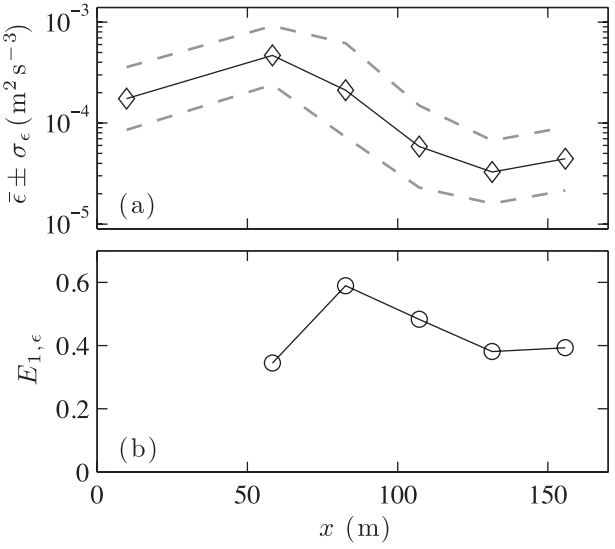

FIG. 3. (a) Mean dissipation rate $\bar{\epsilon}$ (solid line with diamonds) $\pm$ the std dev σ_ϵ (dashed lines) and (b) the first EOF of $\log_{10}(\epsilon)$ $E_{1,\epsilon}$ vs x. In (b) $E_{1,\epsilon}$ is calculated for F3–F7, describing 86% of the variance with $N = 168$.

The time and cross-shore covariability of ϵ is examined with an empirical orthogonal function (EOF) analysis (compactly reproducing the greatest amount of variance) of $\log(\epsilon)$,

$$\log[\epsilon(x_j,t)] = \log[\bar{\epsilon}(x_j)] + \sum_{i=1}^{M} a_{i,\epsilon}(t)E_{i,\epsilon}(x_j),$$

where x_j is the cross-shore frame locations and $E_{i,\epsilon}$ and $a_{i,\epsilon}$ are the EOFs and amplitudes, respectively. The EOF analysis is performed using F3–F7, resulting in $N = 186$ (out of 800) data points (times when ϵ could be estimated at each of F3–F7). F1 is not included because it has few good ϵ estimates, which would severely reduce N. The first EOF $E_{1,\epsilon}(x_j)$ describes 86% of the $\log(\epsilon)$ variance (Fig. 3b), indicating that ϵ variability is largely coherent across the array. The $E_{1,\epsilon}$ is relatively constant at F6 and F7; increases approximately 50% to a F4 maximum, where wave breaking was generally strongest; and at F3 is reduced to offshore levels. The first EOF amplitude $a_{1,\epsilon}$ is related to the incident H_s ($r = 0.61$), inversely to the tide level ($r = -0.45$), and also with F3 $|V|$ ($r = 0.35$; similar for $|V|^3$), demonstrating the complexity in describing the ϵ variability (although of course incident H_s and V are also related).

4. Cross-shore-integrated alongshore momentum and energy balance

a. Alongshore momentum balance

Cross-shore-integrated alongshore momentum balances (e.g., Feddersen et al. 1998) are used to determine if conditions are quasi-alongshore uniform and to estimate bed friction velocity u_* with a least squares best-fit drag coefficient c_d. In nearshore regions, the alongshore bottom stress $\tau_y^b = \rho u_*^2$ often is represented by a quadratic drag law: that is,

$$\tau_y^b = \rho c_d \langle |\mathbf{u}| v \rangle. \tag{6}$$

With alongshore uniformity, a constant c_d, and negligible turbulent cross-shore flux of alongshore momentum at x_{F7}, the cross-shore-integrated alongshore momentum balance is between the alongshore wave and wind forcing and the alongshore bottom stress: that is,

$$\rho^{-1}(-S_{xy}|_{x_{F7}} + \tau_y^{\mathrm{wind}} x_{F7}) = c_d \int_0^{x_{F7}} \langle |\mathbf{u}| v \rangle \, dx, \tag{7}$$

where the off-diagonal radiation stress term S_{xy} is evaluated at the most offshore site F7 and τ_y^{wind} is the alongshore wind stress derived from an anemometer <1 km away. The $\langle |\mathbf{u}| v \rangle$ integral is estimated using the trapezoidal rule, requiring at least four frames with good data for a particular hour (763 out of 800 data runs passed this criterion). On the left-hand side of (7), the rms wind forcing is small (8%) relative to the rms wave forcing. The momentum balance [(7)] closes with high skill (squared correlation of $r^2 = 0.77$) and a least squares best-fit $c_d = 2.3 \times 10^{-3}$ (Fig. 4), which is consistent with previous surf-zone alongshore momentum balances and best-fit c_d (Feddersen et al. 1998; Feddersen and Guza 2003). This suggests that conditions are quasi-alongshore uniform and that u_* can be estimated via (6) with the best-fit c_d.

b. Energy balance

Waves approaching the surf zone have an associated onshore wave energy flux F that is conserved until wave breaking begins. Because $F = 0$ at the shoreline, the incoming wave energy must be converted into other forms of energy within the surf zone. In the simplest steady-state energy balance, the incident wave energy flux is balanced by the depth-integrated turbulent dissipation over the entire surf zone. If dissipation were to be depth uniform, then the simple cross-shore-integrated energy balance between the incident wave energy flux and surf-zone dissipation becomes

$$\int_0^{x_b} h\epsilon \, dx = F_{x_{F7}}. \tag{8}$$

The dissipation rate ϵ varies over the vertical (e.g., GFG), and surf-zone laboratory experiments indicate the majority of dissipation occurs above trough level (e.g., Govender et al. 2004). Thus, the assumption that

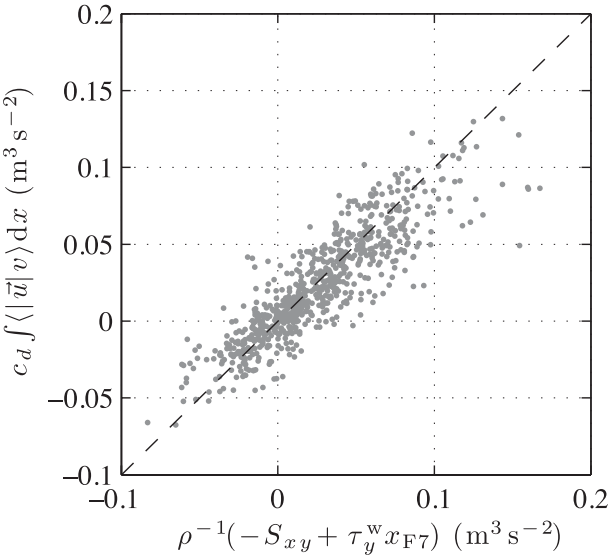

FIG. 4. Cross-shore-integrated alongshore momentum balance (7): $c_d \int_0^{x_{\mathrm{F7}}} \langle |\mathbf{u}| v \rangle \, dx$ vs frame F7 $\rho^{-1}(-S_{xy}|_{x_{\mathrm{F7}}} + \tau_y^{\mathrm{wind}} x_{\mathrm{F7}})$ for at least four good frames. The dashed line is the 1:1 curve. The squared correlation is $r^2 = 0.77$, and the least squares best-fit $c_d = 2.29 \times 10^{-3}$.

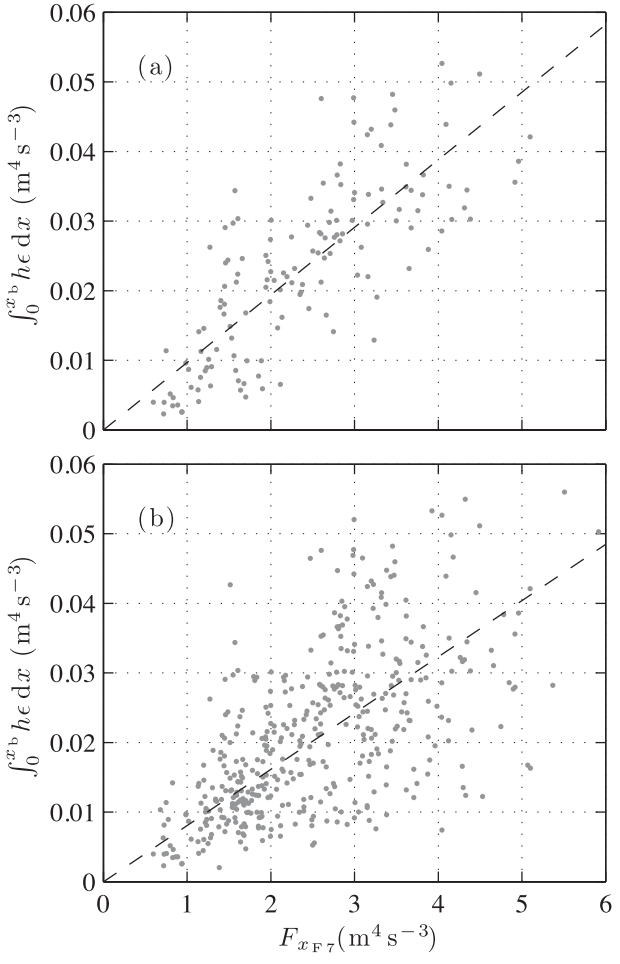

FIG. 5. Cross-shore-integrated energy balance: $\int_0^{x_b} h\epsilon \, dx$ vs incident F7 wave energy flux $F_{x_{\mathrm{F7}}}$ for $\int_0^{x_b} h\epsilon \, dx$ calculated when (a) all surf-zone ϵ values are good ($N = 143$) and (b) at least two (x_b at F3 or F4) or three (if x_b is at F5 or F6) surf-zone ϵ values are good ($N = 430$). The black dashed line represents the least squares best fit constrained to go through the origin with the best-fit slope c and squared correlation r^2 of (a) $c = 0.01$ and $r^2 = 0.61$ and (b) $c = 0.008$ and $r^2 = 0.35$, respectively.

$\int \epsilon(z) \, dz = h\epsilon$ is not appropriate. However, the observed $h\epsilon$ likely is proportional to the depth-integrated dissipation (e.g., Trowbridge and Elgar 2001), particularly as ϵ covaries across the array (Fig. 5). Therefore, the balance $\int h\epsilon \, dx = cF_{x_{\mathrm{F7}}}$ [similar to Eq. (8)] is examined where c is a fit constant of proportionality.

Because of data gaps, $\int_0^{x_b} h\epsilon \, dx$ is calculated in two manners: The first only estimates the integral when all surf-zone frames have good ϵ estimates resulting in $N = 143$ data points. The second requires at least two (for x_b at F3 or F4) or three (for x_b at F5 or F6) good surf-zone ϵ values to calculate the integral resulting in $N = 430$ data points.

The integrated surf-zone dissipation $\int_0^{x_b} h\epsilon \, dx$ using either estimator is linearly related to the incoming wave energy flux $F_{x_{\mathrm{F7}}}$ (Fig. 5), demonstrating the link between incoming wave energy and viscous dissipation to heat, but $\int_0^{x_b} h\epsilon \, dx$ is two orders of magnitude smaller than $F_{x_{\mathrm{F7}}}$ (Fig. 5). With the first $\int_0^{x_b} h\epsilon \, dx$ estimate ($N = 143$), the relationship between $F_{x_{\mathrm{F7}}}$ and $\int_0^{x_b} h\epsilon \, dx$ has moderately high squared correlation $r^2 = 0.61$ with least squares best-fit slope of $c = 0.01$ (Fig. 5a), indicating that only 1% of the depth-normalized wave energy is observed. Using the second $\int_0^{x_b} h\epsilon \, dx$ estimator, with 3 times the number of good data points ($N = 430$), the relationship is similar but noisier, with squared correlation $r^2 = 0.35$ and slope of $c = 0.008$ (Fig. 5b).

5. Local dissipation scalings

Although at each frame the ADV measures ϵ at only a single vertical location, this vertical measurement location varies with time because of tides and bathymetry evolution. This allows the vertical structure of local ϵ scalings to be studied both within and seaward of the surf zone. These scalings implicitly assume a balance of local processes and require quasi-alongshore uniform conditions (as suggested by the alongshore momentum balance closure; Fig. 4) so that ϵ is not driven by alongshore gradients in TKE advection.

a. Surf-zone (Froude) scaling

Nondimensional surf-zone dissipation scaling is developed by normalizing ϵ by the depth-normalized wave energy flux gradient: that is,

$$\frac{\epsilon}{h^{-1}dF/dx}. \tag{9}$$

In a self-similar surf zone (where $\gamma = H_s/h$ is constant) with normally incident narrowband random waves, (9) simplifies to $C^{-1}\epsilon/(g^3h)^{1/2}$, where $C = (5/16)\gamma^2 dh/dx$ and $\epsilon/(g^3h)^{1/2}$ is the surf-zone-scaled ϵ (Feddersen and Trowbridge 2005). Alternatively, this scaling can be similarly nondimensionalized (denoted Froude scaling) assuming $\epsilon \propto u^3/l$ (e.g., Launder and Spalding 1972) using $(gh)^{1/2}$ and h for u and l, respectively (George et al. 1994). Although the scaling has no depth dependence, the surf-zone-scaled $\epsilon/(g^3h)^{1/2}$ observations of GFG and BBG collapsed as a function of z/h (Feddersen and Trowbridge 2005), indicating that, although the depths and wave heights varied, both observed a comparable fraction of depth-normalized lost wave energy ($h^{-1}dF/dx$).

As the surf-zone scaling requires a self-similar surf zone, the scaling is applied to locations at least one frame shoreward of the x_b location so that a self-similar bore can develop. The majority of HB06 surf-zone $\epsilon/(g^3h)^{1/2}$ values fall between 10^{-5} and 10^{-4} (Fig. 6), which is smaller than but largely consistent with prior field observations (GFG; BBG) in the same depth range. HB06 surf-zone $\epsilon/(g^3h)^{1/2}$ values do not extend as far up in the water column as prior field observations because the ϵ QC results in observations rejected at $z/h > 0.6$ (Feddersen 2010). The seaward of the surf-zone $\epsilon/(g^3h)^{1/2}$ values are generally a factor of 10–50 smaller than surf-zone values (not shown). Observed surf-zone $\epsilon/(g^3h)^{1/2}$ increases with z/h, suggesting a breaking-wave-generated turbulence source. Within the vertical range $0.2 < z/h < 0.5$, the surf-zone observed $\epsilon/(g^3h)^{1/2}$ is roughly consistent with laboratory $\epsilon/(g^3h)^{1/2} \approx 1$–$2$ ($\times 10^{-4}$) (e.g., Ting and Kirby 1996; Govender et al. 2004; Huang et al. 2009; Yoon and Cox 2010). With typical beach slopes and γ, the constant $C \approx 10^{-3}$, indicating that, for the observed $\epsilon/(g^3h)^{1/2}$ range, only 1%–10% of the depth-averaged dissipation is observed, which is consistent with the cross-shore-integrated energy balance (Fig. 5).

b. Terray scaling

Although the surf-zone (or Froude) scaling is useful for comparing various field and laboratory surf-zone ϵ observations, it does not provide a vertical dependence or give insight into the water-column turbulent energetics. The deep-water whitecapping-breaking Terray et al. (1996) ϵ scaling (3) is modified for surf-zone depth-limited breaking by setting the surface TKE flux to wave energy flux gradient dF/dx. This assumes that all of the lost wave energy is locally converted to turbulence and not transported onshore by another process, such as

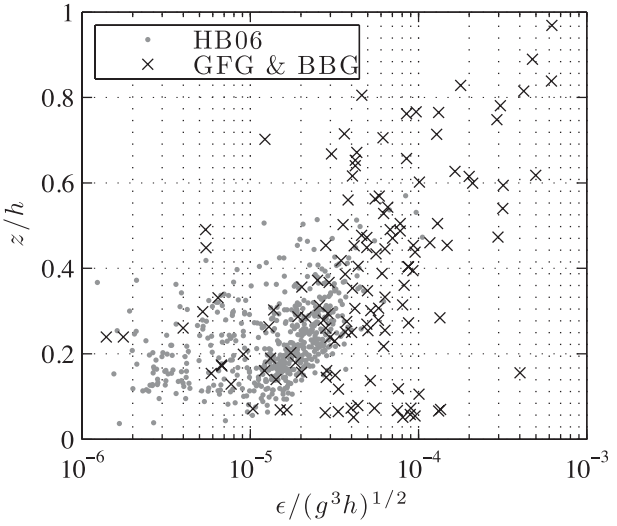

FIG. 6. Surf-zone-scaled dissipation $\epsilon/(g^3h)^{1/2}$ as a function of z/h for HB06 surf zone (gray dots) and previous surf-zone observations (black x) of GFG and BBG.

wave rollers, before conversion to turbulence. Thus, the nondimensional surf-zone Terray ϵ scaling becomes

$$\frac{\epsilon H_s}{dF/dx} = A\left(\frac{z'}{H_s}\right)^{\lambda}, \tag{10}$$

where A and λ are constants. Note that dF/dx is typically two orders of magnitude larger than the inferred whitecapping-induced surface flux just seaward of the surf zone (Feddersen et al. 2007).

The Terray scaling [(10)] has no skill [$r^2 < 0.01$; squared correlation between log of $\epsilon H_s/(dF/dx)$ and z'/H_s] when applied to all surf-zone ϵ observations spanning the entire water column (Fig. 7a) and clearly is not applicable en masse over the entire surf zone. Just seaward of the surf zone, a whitecapping Terray scaling collapsed nondimensional ϵ observations at instruments at locations $0.35 < z/h < 0.65$ but not at instruments close to the bed, $z/h < 0.2$ (Feddersen et al. 2007). Therefore, these surf-zone observations are separated into lower $z/h < 0.25$ and mid $z/h > 0.25$ water-column regions (recall maximum $z/h \approx 0.6$; Fig. 6). Within the lower water column, the Terray scaling [(10)] also has no skill across all surf-zone locations ($r^2 < 0.01$; red dots in Fig. 7b) or at individual locations, analogous to the seaward of the surf-zone results at $z/h < 0.2$ (Feddersen et al. 2007). In the mid-water-column region, the skill ($r^2 = 0.16$) is also small.

The Terray scaling is individually applicable at certain surf-zone locations in the mid water column (Fig. 7c). At F5 and F4, the relationship in (10) has high skill: squared correlation of $r^2 = 0.57$ and $r^2 = 0.63$ with least squares

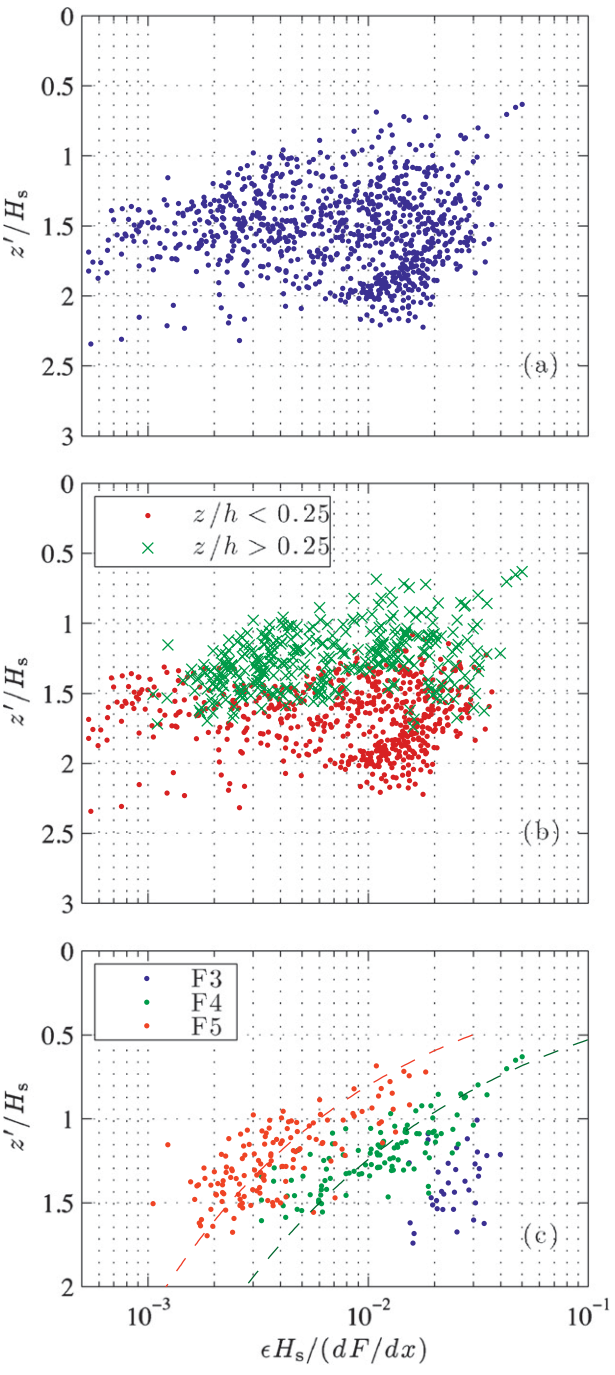

FIG. 7. Terray-scaled $\epsilon H_s/(dF/dx)$ against z'/H_s for (a) surf-zone observations ($N = 934$; $r^2 < 0.01$); (b) all surf-zone observations separated into (see legend) lower-water-column $z/h < 0.25$ ($N = 615$; $r^2 < 0.01$) and mid-water-column $z/h > 0.25$ ($N = 319$; $r^2 = 0.16$); and (c) surf-zone observations for $z/h > 0.25$ at F3, F4, and F5 (see legend) In (c), F3 has $N_{\text{high}} = 34$ and is not fit. The Terray scaling fits (dashed curves) yield $\lambda = -2.68 \pm 0.2$, $A = 0.018 \pm 0.001$, $r^2 = 0.63$, and $N_{\text{high}} = 113$ for F4 (green dashed curve) and $\lambda = -2.33 \pm 0.18$, $A = 0.006 \pm 0.0003$, $r^2 = 0.57$, and $N_{\text{high}} = 140$ for F5 (red dashed curve).

best-fit $\lambda = -2.33 \pm 0.18$ and $\lambda = -2.68 \pm 0.2$, respectively (see legend in Fig. 7c). At F3, $N = 34$ is too small with insufficient $\epsilon H_s/(dF/dx)$ and z'/H_s range to accurately perform a fit. At F1, no wave-breaking mid-water-column ϵ passed the QC tests, and only very rarely was F6 considered within the surf zone. The F4 and F5 λ estimates are roughly consistent with each other and are both somewhat consistent with the canonical $\lambda \approx -2$ value found for whitecapping wave breaking (e.g., Terray et al. 1996). However, the Terray scaling [(10)] does not collapse the observations across frames F3–F5 (see separation of F3–F5 observations in Fig. 7c). The best-fit A varies significantly from $A = 0.006 \pm 0.0003$ at F5 to $A = 0.018 \pm 0.001$ at F4. Furthermore, at F3 the $\epsilon H_s/(dF/dx)$ at a particular z'/H_s is larger than at F4.

c. BBL scaling

In addition to the effects of breaking waves, BBL-generated turbulence may significantly contribute to the water-column turbulence. The BBL-scaled dissipation $\epsilon\kappa z/u_*^3$, based on (2), is examined within and seaward of the surf zone. A value of $\epsilon\kappa z/u_*^3 = 1$ indicates BBL-generated turbulence with $P = \epsilon$, and $\epsilon\kappa z/u_*^3 \gg 1$ indicates surface-generated turbulence with $P \ll \epsilon$. At each frame, the friction velocity u_* is estimated from the alongshore bottom stress (6) as $u_*^2 = c_d\langle|\mathbf{u}|v\rangle$, where the best-fit $c_d = 2.3 \times 10^{-3}$ (section 4a). Although the cross-shore bottom stress can also contribute to the total bottom stress and thus u_*, because of the strong vertical structure of the mean cross-shore current (Faria et al. 2000), it is unclear whether a quadratic drag law is applicable for the cross-shore bottom stress τ_x^b. The observed cross-shore mean currents were weak, and, if the cross-shore bottom stress is estimated from a quadratic drag law (6) (i.e., $\tau_x^b/\rho = c_d\langle|u|u\rangle$), the resulting u_* is marginally different (roughly 3%) from that estimated from the alongshore bottom stress alone and is not significant to the results.

Both within and seaward of the surf zone, $\epsilon\kappa z/u_*^3 > 1$ and the values are inversely dependent on the mean alongshore current magnitude $|V|$ (Fig. 8a). At weaker $|V| < 0.1$ m s^{-1}, almost all values of $\epsilon\kappa z/u_*^3 > 10$ both within and seaward of the surf zone. At all $|V|$, $\epsilon\kappa z/u_*^3$ is consistently larger within than seaward of the surf zone (cf. circles and diamonds in Fig. 8a). Within the surf zone, for $|V| > 0.4$ m s^{-1}, $\epsilon\kappa z/u_*^3$ quasi asymptotes to ≈ 3.

The $\epsilon\kappa z/u_*^3$ scaling implicitly includes the vertical measurement location. However, the BBL scaling applicability depends on relative water-column location. The surf-zone $\epsilon\kappa z/u_*^3$ dependence on $|V|$ is examined separately in the lower ($z/h < 0.25$) and the mid ($z/h > 0.25$) water column. Within the surf zone, the lower-water-column binned-mean $\epsilon\kappa z/u_*^3$ is less than or equal

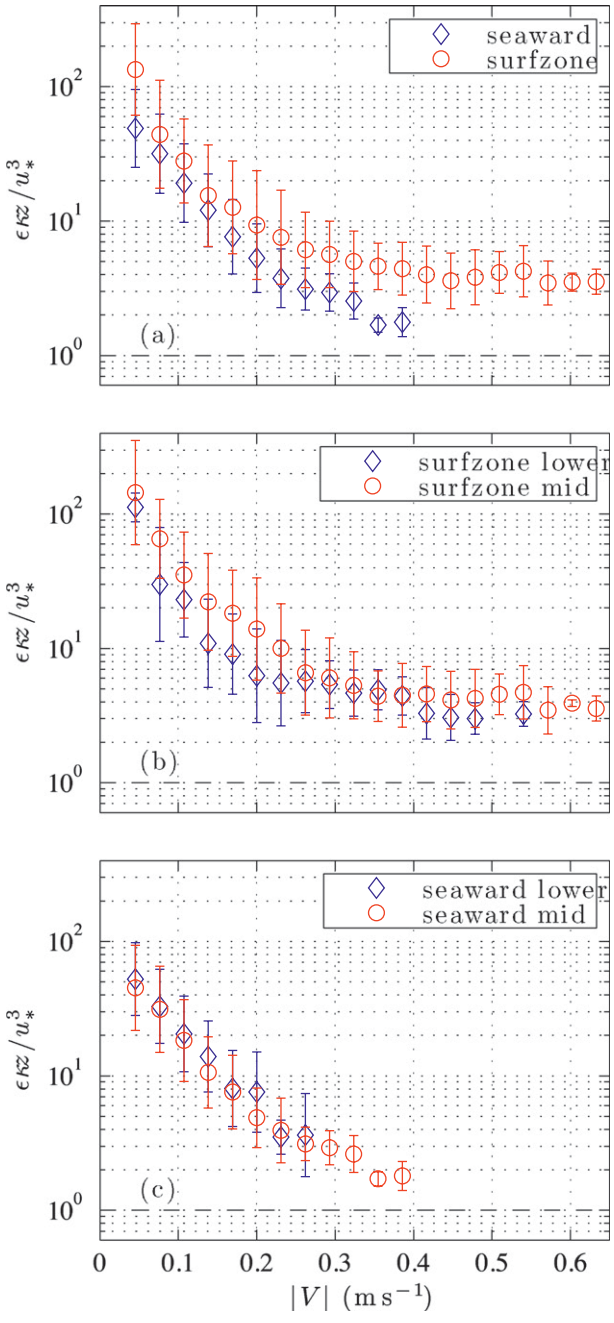

FIG. 8. Nondimensional BBL scaling: binned mean and std dev of $\epsilon\kappa z/u_*^3$ vs mean alongshore current magnitude $|V|$ at (a) locations seaward of (blue with diamonds) and within (red with circles) the surf zone, (b) the surf zone, and (c) seaward of the surf-zone locations. The horizontal dashed–dotted line represents $\epsilon\kappa z/u_*^3 = 1$. In (b) and (c), measurements in the lower ($z/h < 0.25$; blue with diamonds) and mid ($z/h > 0.25$; red with circles) water column are shown.

to the mid-water-column values (Fig. 8b). Seaward of the surf zone, $\epsilon\kappa z/u_*^3$ has a similar $|V|$ dependence for the lower and mid water columns (Fig. 8c). At smaller $|V| <$ 0.15 m s^{-1}, the binned-mean $\epsilon\kappa z/u_*^3 > 10$.

d. Production–dissipation balance at frame F5

The $\epsilon\kappa z/u_*^3$ scaling is based upon shear production balancing dissipation in a classic bottom boundary layer scenario. A direct examination of the ϵ to shear production P ratio is a more robust test of this balance. The shear production P is defined as the product of the Reynolds stress term $\langle v'w' \rangle$ and the vertical shear of the mean alongshore current: that is,

$$P = \langle v'w' \rangle \frac{\partial V}{\partial z}, \tag{11}$$

where the cross-shore production terms were small and neglected.

At F5, the vertical velocity shear $\partial V/\partial z$ was estimated from the Aquadopp velocity profiler interpolated to the vertical location of the ADV, which varied between 0.6 and 0.9 m above the bed. The total water depth was on average 2 m but was as low as $h = 1.5$ m and as large as $h = 3.25$ m. To reduce noise in the $\partial V/\partial z$ estimates, ADCP V values were reconstructed with an first-EOF-based V that was highly correlated ($r^2 > 0.99$) with best-fit slope of 0.99 to the observed V in the first four velocity bins. The ADCP-observed velocity shear magnitude $|\partial V/\partial z|$ decreases with height above the bed. The Reynolds stress was estimated as the friction velocity squared, implicitly assuming a constant stress layer, resulting in the estimated $P = u_*^2 \partial V/\partial z$.

Depending on the incident waves, F5 was located both within or seaward of the surf zone. The binned-mean ϵ/P values have a similar inverse $|V|$ dependence to $\epsilon\kappa z/u_*^3$ (diamonds in Fig. 9). At weak $|V| < 0.1$ m s^{-1}, binned-mean $\epsilon/P > 10$, indicating that BBL-generated turbulence is negligible. However, for stronger currents binned-mean ϵ/P is reduced and approaches an asymptote of $\epsilon/P \approx 2$ for $|V| > 0.3$ m s^{-1}. There is scatter in individual data points, which can be large at small $|V|$ (note the logarithmic scale for ϵ/P in Fig. 9). At a particular $|V|$, ϵ/P is somewhat larger within the surf zone relative to seaward of the surf zone (cf. gray crosses with red dots in Fig. 9). However, the difference is marginal and the number of data points is insufficient to calculate meaningful surf zone and seaward of the surf-zone binned means.

6. Discussion

That $\int_0^{x_b} h\epsilon \, dx$ is correlated with only ≈1% of the incident wave energy flux $F_{x_{F7}}$ (Fig. 5) indicates that the majority of TKE dissipation occurs higher in the water column, which is consistent with laboratory experiments of breaking-wave turbulence dynamics (e.g., Govender et al. 2004; Kimmoun and Branger 2007; Huang et al.

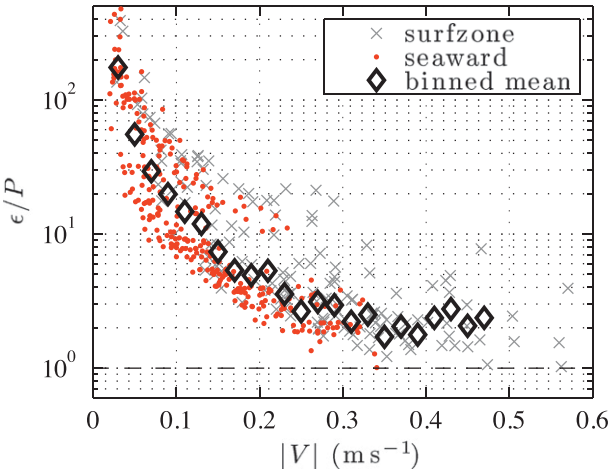

FIG. 9. The ratio ϵ/P vs $|V|$ at F5 for surf zone (×), seaward of the surf zone (red dots), and binned means (black diamonds) for all conditions. Data points with $|V| < 0.03$ m s^{-1} are neglected. There are $N = 486$ (out of 800) hourly observations with 1/3 within and 2/3 seaward of the surf zone. The diamonds represent the binned means for all (both within and seaward of the surf zone) cases. The dashed–dotted line represents $\epsilon/P = 1$.

2009). Laboratory experiments with vertically resolved $\epsilon(z)$ observations find that the $\int \epsilon(z)\,dz$ vertically integrated from the bed through the crest is no more than 10% of the wave energy flux gradient dF/dx (Govender et al. 2004; Huang et al. 2009). Vertically integrating only below trough level yields no more than 2% of dF/dx (Govender et al. 2004), which is consistent with field observations (Fig. 5).

The reasons why even the laboratory vertically integrated ϵ values are such a small fraction of dF/dx are unclear. The incident wave energy is approximately equipartitioned between kinetic and potential energy. With wave breaking, the lost wave energy not only generates turbulence but also raises the potential energy via the bubble-induced void fraction (e.g., Mori et al. 2007). In a laboratory surf zone, the average void fraction above trough level (inferred as large as 0.4) is significant enough to induce a mismatch in the time-averaged cross-shore volume flux (Govender et al. 2002; Kimmoun and Branger 2007). Work must be performed by the wave field to maintain the elevated void fraction levels. Furthermore, the void-fraction-induced buoyancy flux may inhibit the vertical diffusion of TKE to the region below trough level. Therefore, only a fraction (<1) of the incident wave-energy flux is expected to be available as a surface TKE flux.

In the lower water column ($z/h < 0.25$), the Terray scaling's [(10)] lack of skill is potentially a result of bottom boundary layer processes (shear production) becoming important and the sea-bed boundary preventing the turbulent length scale from continuing to grow below the surface (e.g., Feddersen et al. 2007). The observed mid-water-column Terray-scaling (Fig. 7c) λ values at F4 ($\lambda = -2.68 \pm 0.18$) and F5 ($\lambda = -2.33 \pm 0.2$) are roughly consistent with values found in intermediate-depth whitecapping wave breaking studies. Seaward of the surf zone in 3.5-m mean depth, Feddersen et al. (2007) found $\lambda = -1.9$, and, in a shallow estuary, Jones and Monismith (2008a) found $\lambda = -2.2$. In 12-m depth, Gerbi et al. (2009) did not fit λ, but, from their observations, a best-fit λ would be <-2. This indicates that, in the surf-zone mid water column, the turbulence processes under depth-limited breaking waves are similar to under whitecapping breaking waves.

The Terray scaling [(10)] does not collapse the mid-water-column observations across all surf-zone frames (Fig. 7b), because of variation in the best-fit A [(10)]. However, the linear wave energy flux gradient dF/dx may not be proportional to the surface TKE flux in (10), which may induce the A variation. In a laboratory surf zone, the ratio $\int \epsilon\,dz/(dF/dx)$ varied in the cross-shore with a minimum (≈0.02) at wave breaking and became maximum (≈0.1) farther onshore once a self-similar bore had developed (Huang et al. 2009). This suggests that dF/dx may not accurately represent the surf-zone surface TKE flux. One possibility is that the lost wave energy (dF/dx) is converted into an intermediary form such as a wave roller (e.g., Stive and de Vriend 1994) that is advected onshore before converting into a surface TKE flux. This would induce a cross-shore lag between dF/dx and the surface TKE flux and could explain why the laboratory ratio $\int \epsilon\,dz/(dF/dx)$ varied in the cross-shore. This pattern of laboratory $\int \epsilon\,dz/(dF/dx)$ is consistent with the cross-shore pattern of Terray-scaling best-fit A, which increases toward the shore (at F5 $A = 0.006$, at F4 $A = 0.0018$, and at F3 it would be larger still; Fig. 7c). In addition, within the surf zone, the linear estimator for the wave energy flux and the finite difference introduces error in the dF/dx estimates, analogous to the uncertainties in the wind friction velocity-based parameterizations for the surface TKE flux in regions seaward of the surf zone (Feddersen et al. 2007; Jones and Monismith 2008a; Gerbi et al. 2009). In a laboratory surf zone with small 3-cm incident waves (Huang et al. 2009), the linear-theory-estimated F was qualitatively similar to, albeit at times 50% larger than, the directly estimated (by vertically integrating the velocities) F. Therefore, with a more appropriate surface TKE flux measure, the Terray scaling potentially could collapse mid-water-column ϵ observations in the mid to outer surf zone.

When the surf-zone alongshore current is strong ($|V| > 0.3$ m s^{-1}), the binned mean $\epsilon\kappa z/u_*^3 < 5$ (Figs. 8a,b), suggesting that BBL processes also significantly contribute to

the surf-zone water-column turbulence. Within the surf zone, the smaller lower-water-column $\epsilon\kappa z/u_*^3$ (Fig. 8b), where the Terray breaking-wave scaling does not work (Fig. 7b), indicates that vertical TKE diffusion is weaker and that P is closer to ϵ, relative to the mid water column. The u_* estimated with a quadratic drag law and a (time and cross-shore) constant c_d may have some error. Inverse estimates of surf-zone c_d indicate that c_d could vary by 33% across the surf zone (Feddersen et al. 2004), with a potential 50% variation in u_*^3. Furthermore, the surf-zone turbulent length scale may deviate from a classic BBL $l = \kappa z$ because of the mix of turbulence processes. Given this uncertainty, the fact that the surf-zone $\epsilon\kappa z/u_*^3$ asymptotes at larger $|V|$ (>0.4 m s^{-1}) to a quasi-constant value (Fig. 8a) suggests that $P \approx \epsilon$, as the binned-mean $\epsilon\kappa z/u_*^3$, does not continue to decrease with larger $|V|$. This is supported by the surf-zone F5 asymptoted binned-mean $\epsilon/P \approx 2-3$ (Fig. 9) when $|V| > 0.3$ m s^{-1}. The $\epsilon\kappa z/u_*^3$ asymptote together with lower values in the lower water column indicates that BBL can be the dominant turbulence source in the lower water column when $|V|$ is strong (>0.4 m s^{-1}).

That $\epsilon\kappa z/u_*^3$ is closer to unity seaward than within of the surf zone (Fig. 8a) and that seaward of the surf-zone $\epsilon\kappa z/u_*^3$ does not depend on water column location (Fig. 8c) suggest that BBL turbulent energetics are more applicable over more of the water column when waves are not breaking. Another possibility is that the appropriate seaward of the surf-zone c_d (used to estimate u_*) is smaller than within the surf zone (e.g., Feddersen et al. 1998), and, by using the larger best-fit c_d to estimate u_*, this could bias the seaward of the surf-zone $\epsilon\kappa z/u_*^3$ estimates toward lower values. At weak $|V| < 0.15$ m s^{-1}, the large $\epsilon\kappa z/u_*^3$ and F5 ϵ/P indicate that other processes such as whitecapping wave breaking (Feddersen et al. 2007) or cross-shore turbulent transport from the surf zone could be leading to the seaward of the surf-zone departure from BBL scaling.

The SBL and BBL turbulence generation mechanisms are not independent, with both depending upon the incident wave field. For simple alongshore uniform beaches, the wave-driven alongshore currents result from a balance between gradients of the off-diagonal radiation stress component and the bottom stress: that is, $-\rho^{-1}dS_{xy}/dx = u_*^2$ (e.g., Longuet-Higgins 1970a,b). For narrowbanded random waves, the alongshore wave forcing is given by $\rho^{-1}dS_{xy}/dx = dF/dx[\sin(\theta_0)/c_0]$ (e.g., Thornton and Guza 1986) ,where c_0 and θ_0 are the incident (outside the surf zone) phase speed and wave angle, respectively, using $\sin(\theta)/c$ conservation (Snell's law). A purely BBL-scaled $\epsilon_{\rm BBL}(z) = [\sin(\theta_0)/c_0]^{3/2}(dF/dx)^{3/2}/(\kappa z)$, and the purely Terray-scaled dissipation $\epsilon_{\rm SBL}(z') = A(dF/dx)H_s^{-1}(z'/H_s)^{\lambda}$. The dependence of $\epsilon_{\rm BBL}$ on dF/dx explains how $\int h\epsilon\, dx$ can be related to $F_{x_{\rm F7}}$ (Fig. 5), even if a significant portion of the turbulence is generated within the BBL. Within a self-similar surf zone (where $\gamma = H_s/h$), the ratio $\epsilon_{\rm BBL}/\epsilon_{\rm SBL}$ at a relative water-column position $z = \delta h$ can be crudely estimated as

$$\frac{\epsilon_{\rm BBL}}{\epsilon_{\rm SBL}} = \frac{(\sin\theta_0/c_0)^{3/2}(5/16)^{1/2}g^{3/4}h^{3/4}(dh/dx)^{1/2}\gamma^{2-\lambda}}{A\kappa\delta(1-\delta)^{\lambda}}, \quad (12)$$

where $dF/dx = (5/16)\gamma^2 g^{3/2}h^{3/2}dh/dx$ (assuming $\cos\theta \approx 1$) is used. The ratio (12) has a complex dependence upon a number of factors. If $A, \lambda, \gamma, dh/dx$ (i.e., planar beach), and δ are fixed, then the ratio in (12) depends almost linearly on depth ($h^{3/4}$) and on incident wave angle θ_0. Thus, surf-zone BBL-generated turbulence will be relatively more important in deeper surf zones with larger angles of incidence as occurred when the observations of Trowbridge and Elgar (2001) were within the surf zone (Feddersen and Trowbridge 2005). Note that in the laboratory $\theta_0 = 0$ and that there is no BBL-generated turbulence.

In analogy with grid stirring experiments (e.g., Thompson and Turner 1975), the SBL Terray scaling can be reproduced by two-equation turbulence models such as the k–ϵ (e.g., Burchard 2001) and k–ω (e.g., Umlauf et al. 2003). A solution to these models is $d/dz(\nu dk/dz) = \epsilon$ with turbulence length scale increasing linearly with depth below the surface $l = \beta z' + l_s$, where l_s is typically set equal to some fraction of the wave height H_s (e.g., Jones and Monismith 2008b), and $\beta \approx 0.25$ (for k–ω model). Two-equation turbulence models also can reproduce the BBL scaling where $P = \epsilon$ and the turbulent length scale $l \propto \kappa z$. At some vertical location, these surface and bottom length scales overlap (e.g., Feddersen et al. 2007; Jones and Monismith 2008a), which depends upon geometry and upon the surface TKE flux magnitude and u_*. In 3.5-m depth seaward of the surf zone under whitecapping conditions, the near-bed $P \ll \epsilon$, but the Terray scaling [(3)] was not applicable, likely because of a near-bed decrease in the turbulent length scale (Feddersen et al. 2007). Therefore, even if BBL ($P = \epsilon$) or SBL [$d/dz(\nu dk/dz) = \epsilon$] turbulent energetics apply locally, the BBL [(2)] or Terray [(10)] scalings may not apply locally because the turbulent length scale l may not follow the scaling's assumptions. A vertical array of ϵ and P measurements is required to properly diagnose the surf-zone water-column turbulent energetics and to test two-equation turbulence models for the surf zone.

7. Summary

Field observations of the turbulent dissipation rate ϵ from a cross-shore transect of instruments spanning the surf zone are reported. Measured surf-zone ϵ values range 10^{-4} to 10^{-3} m^2 s^{-3} and are typically a factor of 10 larger than seaward of the surf zone. Across the

array, ϵ covaried significantly with the first EOF of ϵ describing 88% of the variance. The ϵ variability was complex, correlated with incident wave height, the alongshore current magnitude, and inversely to the tide level. Cross-shore-integrated alongshore momentum balances closed indicating quasi-alongshore uniform conditions and providing a method to estimate u_*. The cross-shore-integrated $h\epsilon$ was correlated with but with only 1% of the incident wave energy flux, which is consistent with the amount of laboratory ϵ observed in the water column.

Local dissipation scalings were subsequently examined. Surf-zone-scaled $\epsilon/(g^3h)^{1/2}$ values were largely consistent with previous observations and roughly consistent with (although less than) laboratory observations. In the mid water column, a surf-zone Terray scaling (adapted from the deep-water scaling) was applicable at mid to outer surf-zone locations. However, the scaling constant A varied in the cross-shore, preventing the scaling from collapsing across locations. This cross-shore variation in A was consistent with laboratory observations of the ratio $(\int \epsilon\, dz)/(dF/dx)$, possibly suggesting a cross-shore lag between wave energy gradients and surface flux of TKE. Bottom boundary layer (BBL)-scaled dissipation $\epsilon\kappa z/u_*^3$ had a strong alongshore current dependence. With stronger alongshore currents ($|V| > 0.4$ m s^{-1}), $\epsilon\kappa z/u_*^3$ asymptotes at $\approx$3, indicating that, particularly in the lower water column, BBL-generated turbulence can be a dominant turbulence source when currents are strong. This turbulence generation mechanism is not present in laboratory surf-zone turbulence studies.

In general, surf-zone turbulence is due to a combination of surface (wave breaking) and bottom (current shear) processes. This combination of scalings is complex, but generally BBL-generated turbulence will be stronger in deeper surf zones with larger incident wave angles. However, examining the surface scalings in isolation assumes particular turbulent length scale depth variations, which are not applicable over the entire water column. To more deeply diagnose the surf-zone water-column turbulence energetics, a vertical array of turbulence measurements is required.

Acknowledgments. The HB06 experiment and this research were supported by CA Coastal Conservancy, NOAA, ONR, NSF, and CA Sea Grant. R. T. Guza was co-PI on the HB06 experiment. Staff and students from the Integrative Oceanography Division (B. Woodward, B. Boyd, K. Smith, D. Darnell, I. Nagy, D. Clark, M. Omand, M. Okihiro, M. Yates, M. McKenna, M. Rippy, S. Henderson, and M. Spydell) were instrumental in acquiring the field observations for this research. Two anonymous referees helped improve this work.

REFERENCES

Agrawal, Y. C., E. A. Terray, M. A. Donelan, P. A. Hwang, A. J. Williams, W. M. Drennan, K. K. Kahma, and S. A. Kitaigorodskii, 1992: Enhanced dissipation of kinetic-energy beneath surface-waves. *Nature,* **359,** 219–220.

Bryan, K. R., K. P. Black, and R. M. Gorman, 2003: Spectral estimates of dissipation rate within and near the surf zone. *J. Phys. Oceanogr.,* **33,** 979–993.

Burchard, H., 2001: Simulating the wave-enhanced layer under breaking surface waves with two-equation turbulence models. *J. Phys. Oceanogr.,* **31,** 3133–3145.

Chang, K., and P. Liu, 1999: Experimental investigation of turbulence generated by breaking waves in water of intermediate depth. *Phys. Fluids,* **11,** 3390–3400.

Clark, D. B., F. Feddersen, and R. T. Guza, 2010: Cross-shore surfzone tracer dispersion in an alongshore current. *J. Geophys. Res.,* **115,** C10035, doi:10.1029/2009JC005683.

Craig, P. D., and M. L. Banner, 1994: Modeling wave-enhanced turbulence in the ocean surface layer. *J. Phys. Oceanogr.,* **24,** 2546–2559.

Dewey, R. K., and W. R. Crawford, 1988: Bottom stress estimates from vertical dissipation rate profiles on the continental shelf. *J. Phys. Oceanogr.,* **18,** 1167–1177.

Drennan, W. M., M. A. Donelan, E. A. Terray, and K. B. Katsaros, 1996: Oceanic turbulence dissipation measurements in SWADE. *J. Phys. Oceanogr.,* **26,** 808–815.

Elgar, S., B. Raubenheimer, and R. T. Guza, 2005: Quality control of acoustic Doppler velocimeter data in the surfzone. *Meas. Sci. Technol.,* **16,** 1889–1893.

Faria, A., E. Thornton, T. Lippmann, and T. Stanton, 2000: Undertow over a barred beach. *J. Geophys. Res.,* **105,** 16 999–17 010.

Feddersen, F., 2010: Quality controlling surfzone acoustic Doppler velocimeter observations to estimate the turbulent dissipation rate. *J. Atmos. Oceanic Technol.,* **27,** 2039–2055.

——, and R. T. Guza, 2003: Observations of nearshore circulation: Alongshore uniformity. *J. Geophys. Res.,* **108,** 3006, doi:10.1029/2001JC001293.

——, and J. H. Trowbridge, 2005: The effect of wave breaking on surf-zone turbulence and alongshore currents: a modelling study. *J. Phys. Oceanogr.,* **35,** 2187–2204.

——, R. T. Guza, S. Elgar, and T. H. C. Herbers, 1998: Alongshore momentum balances in the nearshore. *J. Geophys. Res.,* **103,** 15 667–15 676.

——, ——, and —— , 2004: Inverse modeling of one-dimensional setup and alongshore current in the nearshore. *J. Phys. Oceanogr.,* **34,** 920–933.

——, J. H. Trowbridge, and A. J. Williams, 2007: Vertical structure of dissipation in the nearshore. *J. Phys. Oceanogr.,* **37,** 1764–1777.

George, R., R. E. Flick, and R. T. Guza, 1994: Observations of turbulence in the surf zone. *J. Geophys. Res.,* **99,** 801–810.

Gerbi, G. P., J. H. Trowbridge, E. A. Terray, A. J. Plueddemann, and T. Kukulka, 2009: Observations of turbulence in the ocean surface boundary layer: Energetics and transport. *J. Phys. Oceanogr.,* **39,** 1077–1096.

Govender, K., G. P. Mocke, and M. J. Alport, 2002: Video-imaged surf zone wave and roller structures and flow fields. *J. Geophys. Res.,* **107,** 3072, doi:10.1029/2000JC000755.

——, ——, and ——, 2004: Dissipation of isotropic turbulence and length-scale measurements through the wave roller in laboratory spilling waves. *J. Geophys. Res.,* **109,** C08018, doi:10.1029/2003JC002233.

Grant, W., and O. Madsen, 1979: Combined wave and current interaction with a rough bottom. *J. Geophys. Res.,* **84,** 1797–1808.

Greenan, B., N. Oakey, and F. Dobson, 2001: Estimates of dissipation in the ocean mixed layer using a quasi-horizontal microstructure profiler. *J. Phys. Oceanogr.,* **31,** 992–1004.

Gross, T. F., and A. R. M. Nowell, 1985: Spectral scaling in a tidal boundary layer. *J. Phys. Oceanogr.,* **15,** 496–508.

Huang, Z.-C., S.-C. Hsiao, H.-H. Hwung, and K.-A. Chang, 2009: Turbulence and energy dissipations of surf-zone spilling breakers. *Coastal Eng.,* **56,** 733–746, doi:10.1016/j.coastaleng.2009.02.003.

Jones, N. L., and S. G. Monismith, 2008a: The influence of whitecapping waves on the vertical structure of turbulence in a shallow estuarine embayment. *J. Phys. Oceanogr.,* **38,** 1563–1580.

——, and ——, 2008b: Modeling the influence of wave-enhanced turbulence in a shallow tide- and wind-driven water column. *J. Geophys. Res.,* **113,** C03009, doi:10.1029/2007JC004246.

Kimmoun, O., and H. Branger, 2007: A particle image velocimetry investigation on laboratory surf-zone breaking waves over a sloping beach. *J. Fluid Mech.,* **588,** 353–397, doi:10.1017/S0022112007007641.

Kuik, A. J., G. P. V. Vledder, and L. H. Holthuijsen, 1988: A method for the routine analysis of pitch-and-roll buoy wave data. *J. Phys. Oceanogr.,* **18,** 1020–1034.

Launder, B. E., and D. B. Spalding, 1972: *Mathematical Models of Turbulence*. Academic Press, 169 pp.

Longuet-Higgins, M. S., 1970a: Longshore currents generated by obliquely incident sea waves, 1. *J. Geophys. Res.,* **75,** 6778–6789.

——, 1970b: Longshore currents generated by obliquely incident sea waves, 2. *J. Geophys. Res.,* **75,** 6790–6801.

Lumley, J. L., and E. A. Terray, 1983: Kinematics of turbulence convected by a random wave field. *J. Phys. Oceanogr.,* **13,** 2000–2007.

Mocke, G., 2001: Structure and modeling of surf zone turbulence due to wave breaking. *J. Geophys. Res.,* **106,** 17 039–17 057.

Mori, N., T. Suzuki, and S. Kakuno, 2007: Experimental study of air bubbles and turbulence characteristics in the surf zone. *J. Geophys. Res.,* **112,** C05014, doi:10.1029/2006JC003647.

Nadaoka, K., M. Hino, and Y. Koyano, 1989: Structure of the turbulent-flow field under breaking waves in the surf zone. *J. Fluid Mech.,* **204,** 359–387.

Omand, M. M., J. J. Leichter, P. J. S. Franks, A. J. Lucas, R. T. Guza, and F. Feddersen, 2011: Physical and biological processes underlying the sudden appearance of a red-tide surface patch in the nearshore. *Limnol. Oceanogr.,* **56,** 787–801, doi:10.4319/lo.2011.56.3.0787.

Peters, H., and R. Bokhorst, 2000: Microstructure observations of turbulent mixing in a partially mixed estuary. Part I: Dissipation rate. *J. Phys. Oceanogr.,* **30,** 1232–1244.

Raubenheimber, B., S. Elgar, and R. T. Guza, 1998: Estimating wave heights from pressure measured in a sand bed. *J. Waterw. Port Coastal Ocean Eng.,* **124,** 151–154.

——, ——, and ——, 2004: Observations of swash zone velocities: A note on friction coefficients. *J. Geophys. Res.,* **109,** C01027, doi:10.1029/2003JC001877.

Reidenbach, M. A., S. G. Monismith, J. R. Koseff, G. Yahel, and A. Genin, 2006: Boundary layer turbulence and flow structure over a fringing coral reef. *Limnol. Oceanogr.,* **51,** 1956–1968.

Ruessink, B. G., 2010: Observations of turbulence within a natural surf zone. *J. Phys. Oceanogr.,* **40,** 2696–2712.

Sanford, T., and R. Lien, 1999: Turbulent properties in a homogeneous tidal bottom boundary layer. *J. Geophys. Res.,* **104,** 1245–1257.

Scott, C. P., D. T. Cox, T. B. Maddux, and J. W. Long, 2005: Large-scale laboratory observations of turbulence on a fixed barred beach. *Meas. Sci. Technol.,* **16,** 1903–1912.

Shaw, W. J., J. H. Trowbridge, and A. J. Williams, 2001: Budgets of turbulent kinetic energy and scalar variance in the continental shelf bottom boundary layer. *J. Geophys. Res.,* **106,** 9551–9564.

Sheremet, A., R. T. Guza, and T. H. C. Herbers, 2005: A new estimator for directional properties of nearshore waves. *J. Geophys. Res.,* **110,** C01001, doi:10.1029/2003JC002236.

Soloviev, A., and R. Lukas, 2003: Observation of wave-enhanced turbulence in the near-surface layer of the ocean during TOGA COARE. *Deep-Sea Res. I,* **50,** 371–395, doi:10.1016/S0967-0637(03)00004-9.

Sontek, 2004: Sontek ADVField acoustic Doppler velocimeter: Technical documentation. Sontek/YSI Rep., 186 pp.

Sou, I. M., E. A. Cowen, and P. L. F. Liu, 2010: Evolution of the turbulence structure in the surf and swash zones. *J. Fluid Mech.,* **644,** 193–216, doi:10.1017/S0022112009992321.

Spydell, M. S., F. Feddersen, and R. T. Guza, 2009: Observations of drifter dispersion in the surfzone: The effect of sheared alongshore currents. *J. Geophys. Res.,* **114,** C07028, doi:10.1029/2009JC005328.

Stips, A., H. Burchard, K. Bolding, H. Prandke, A. Simon, and A. West, 2005: Measurement and simulation of viscous dissipation in the wave affected surface layer. *Deep-Sea Res. II,* **52,** 1133–1155, doi:10.1016/j.dsr2.2005.01.012.

Stive, M. J. F., and H. J. de Vriend, 1994: Shear stresses and mean in shoaling and breaking waves. *Proc. 24th Int. Coastal Engineering. Conf.,* Kobe, Japan, ASCE, 594–608.

Terray, E. A., M. A. Donelan, Y. C. Agrawal, W. M. Drennan, K. K. Kahma, A. J. Williams, P. A. Hwang, and S. A. Kitaigorodskii, 1996: Estimates of kinetic energy dissipation under breaking waves. *J. Phys. Oceanogr.,* **26,** 792–807.

Thompson, S., and J. Turner, 1975: Mixing across an interface due to turbulence generated by an oscillating grid. *J. Fluid Mech.,* **67,** 349.

Thornton, E. B., and R. T. Guza, 1983: Transformation of wave height distribution. *J. Geophys. Res.,* **88,** 5925–5938.

——, and ——, 1986: Surf zone longshore currents and randome waves: Field data and models. *J. Phys. Oceanogr.,* **16,** 1165–1178.

——, and C. Kim, 1993: Longshore current and wave height modulation at tidal frequency inside the surf zone. *J. Geophys. Res.,* **98,** 16 509–16 519.

Ting, F. C. K., and J. T. Kirby, 1995: Dynamics of surf-zone turbulence in a strong plunging breaker. *Coastal Eng.,* **24,** 177–204.

——, and ——, 1996: Dynamics of surf-zone turbulence in a spilling breaker. *Coastal Eng.,* **27,** 131–160.

Trowbridge, J. H., and S. Elgar, 2001: Turbulence measurements in the surf zone. *J. Phys. Oceanogr.,* **31,** 2403–2417.

——, W. R. Geyer, M. M. Bowen, and A. J. Williams, 1999: Near-bottom turbulence measurements in a partially mixed estuary: Turbulent energy balance, velocity structure, and along-channel momentum balance. *J. Phys. Oceanogr.,* **29,** 3056–3072.

Umlauf, L., H. Burchard, and K. Hutter, 2003: Extending the k-omega turbulence model towards oceanic applications. *Ocean Modell.,* **5,** 195–218.

Yoon, H.-D., and D. T. Cox, 2010: Large-scale laboratory observations of wave breaking turbulence over an evolving beach. *J. Geophys. Res.,* **115,** C10007, doi:10.1029/2009JC005748.